Application of Double Negative Materials to Increase the Power Radiated by Electrically Small Antennas

Richard W. Ziolkowski, *Fellow, IEEE,* and Allison D. Kipple, *Student Member, IEEE*

***Abstract*—The effect of surrounding an electrically small dipole antenna with a shell of double negative (DNG) material ($\varepsilon_r < 0$ and $\mu_r < 0$) has been investigated both analytically and numerically. The problem of an infinitesimal electric dipole embedded in a homogeneous DNG medium is treated; its analytical solution shows that this electrically small antenna acts inductively rather than capacitively as it would in free space. It is then shown that a properly designed dipole-DNG shell combination increases the real power radiated by more than an order of magnitude over the corresponding free space case. The reactance of the antenna is shown to have a corresponding decrease. Analysis of the reactive power within this dipole-DNG shell system indicates that the DNG shell acts as a natural matching network for the dipole. An equivalent circuit model is introduced that confirms this explanation. Several cases are presented to illustrate these results. The difficult problem of interpreting the energy stored in this dipole-DNG shell system when the DNG medium is frequency independent and, hence, of calculating the radiation Q is discussed from several points of view.**

***Index Terms*—Antenna theory, antennas, complex media, dipole antennas, electrically small antennas, electromagentic fields.**

I. Introduction

DOUBLE NEGATIVE (DNG) materials, i.e., materials with both negative permittivity and negative permeability [for instance, [1]–[3]], have been a topic of high interest in recent years. These materials are typically realized artificially as composite structures that are constructed from arrays of metallic inclusions in dielectric or magnetic substrates, and they exhibit unusual scattering and propagation properties within a particular frequency range. For instance, in contrast to a double positive (DPS) medium, i.e., a normal medium that has both positive permittivity and permeability, the wavenumber $\boldsymbol{k}$ in a DNG material is opposite to, rather than parallel to, the Poynting's vector associated with a plane wave propagating in it. Thus, the Poynting's vector is parallel to, and the wavenumber $\boldsymbol{k}$ is antiparallel to, the direction of causal power flow [3]. The property of interest to the present application involves the possibility that the DNG material could match the intrinsic reactance of an electrically small dipole antenna to free space, hence, provide a natural matching circuit to the antenna.

A comparison of the impedance and associated reactance of an infinitesimal dipole radiating into homogeneous DPS and DNG media is presented in Section II. It is found that the antenna acts inductively in the presence of the DNG medium rather than capacitively as it does in free space. This result suggests that a DNG shell could be used in a natural manner to match the small dipole to free space. The analytical solution to the problem of an infinitesimal electric dipole antenna radiating in the presence of a DNG shell is then discussed in Section III. Numerical analyses of this dipole-DNG shell system, when the DNG medium is dual to free space, are given in Section IV. A substantial increase in the radiated power and a corresponding decrease in the reactance seen by the antenna are demonstrated with a properly designed dipole-DNG shell system. It is shown in Section V that a circuit model of the dipole-DNG shell system can be constructed and that it confirms the matching network concept of the DNG shell. Numerical results for more general dipole-DNG shell systems are considered in Section VI. A discussion of the calculation of the reactance, its interpretation, and its relationships to the radiated power and stored electric and magnetic field energies for the dipole-DNG shell system is given in Section VII. The corresponding nonpropagating field energy calculations of the radiation quality factor Q for the dipole-DNG shell system are discussed in Section VIII. A summary of the results is presented in Section IX.

II. Behavior of an Infinitesimal Dipole in DPS and DNG Media

Let the surface S represent the smallest sphere of radius a that can enclose the dipole. If the dipole has length ℓ, then $a = l/2$. Let V be the volume exterior to that sphere. The surface S together with the surface at infinity, S_∞, is the boundary of V. Let the unit normal $-\hat{n} \equiv \hat{r}$ point into the volume V. The time averaged complex power P flowing through S then takes the form [4]–[11]

$$P = \frac{1}{2} \oiint_S \left[\vec{E}_\omega \times \vec{H}_\omega^*\right] \bullet (-\hat{n})\, dS = P_{\rm rad} + j\, P_{\rm reac} \qquad (1)$$

where $\vec{E}_\omega$ and $\vec{H}_\omega$ represent the time harmonic electric and magnetic fields produced by the dipole, and $P_{\rm rad}$ and $P_{\rm reac}$ represent the time averaged radiated power (real part) and the time averag-ed reactive power (imaginary part), respectively. The latter are given explicitly by the expressions

$$P_{\rm rad} = \frac{1}{2}{\rm Re}\left[\oiint_S \vec{E}_\omega \times \vec{H}_\omega^* \bullet \hat{r}\, dS\right]$$

$$P_{\rm reac} = \frac{1}{2}{\rm Im}\left[\oiint_S \vec{E}_\omega \times \vec{H}_\omega^* \bullet \hat{r}\, dS\right] = 2\omega\,(W_m - W_e) \qquad (2)$$

Manuscript received August 15, 2002; revised February 3, 2003. This work was supported in part by the Kavli Institute for Theoretical Physics through the National Science Foundation under Grant PHY99-07949.

The authors are with the Department of Electrical and Computer Engineering, The University of Arizona, Tucson, AZ 85721 USA (e-mail: ziolkowski@ece.arizona.edu; kipplea@ece.arizona.edu).

Digital Object Identifier 10.1109/TAP.2003.817561

where, if the permittivity ε and permeability μ are uniform and constant throughout V, the time averaged electric and magnetic field energies stored in V are, respectively

$$W_e = \frac{1}{4}\iiint_V \varepsilon \vec{E}_\omega \bullet \vec{E}_\omega^* \, dV$$
$$W_m = \frac{1}{4}\iiint_V \mu \vec{H}_\omega \bullet \vec{H}_\omega^* \, dV. \tag{3}$$

If the average input power to the antenna system is $(1/2)VI^*$, one can write the input impedance for the dipole antenna as $Z = R_{\rm rad} + jX_{\rm ant}$, so that $P_{\rm rad} = (1/2)II^*R_{\rm rad}$ and $P_{\rm reac} = (1/2)II^*X_{\rm ant}$ [4]–[11]. The radiation resistance seen by the antenna is $R_{\rm rad}$; the reactance seen by the antenna is $X_{\rm ant}$. For the discussion here, we then introduce a normalized reactance parameter for the antenna as

$$X_R(a) = \frac{P_{\rm reac}}{P_{\rm rad}} = \frac{X_{\rm ant}}{R_{\rm rad}}. \tag{4}$$

This parameter gives a quantitative estimate for the ratio of the reactance to the resistance of the input impedance of the antenna system as measured at the sphere of radius a. An antenna with a small value of X_R would have desirable performance characteristics, i.e., it would have a small input reactance and a large radiation resistance.

Given the following equations for the time harmonic fields $\vec{E}_\omega$, $\vec{H}_\omega$ radiated by an infinitesimal electric dipole immersed in a conventional double positive (DPS) medium [4, p. 135]

$$H_r = H_\theta = 0 \tag{5}$$
$$H_\phi = j\frac{kI_0 l \sin\theta}{4\pi r}\left[1 + \frac{1}{jkr}\right]e^{-jkr} \tag{6}$$
$$E_r = \eta\frac{I_0 l \cos\theta}{2\pi r^2}\left[1 + \frac{1}{jkr}\right]e^{-jkr} \tag{7}$$
$$E_\theta = j\eta\frac{kI_0 l \sin\theta}{4\pi r}\left[1 + \frac{1}{jkr} - \frac{1}{(kr)^2}\right]e^{-jkr} \tag{8}$$
$$E_\phi = 0 \tag{9}$$

one can find the time averaged complex power P flowing through the surface S around the dipole to be the expression [4, p. 136]

$$P_{DPS} = \eta\frac{\pi}{3}\left|\frac{I_0 l}{\lambda}\right|^2\left[1 - \frac{j}{(ka)^3}\right]. \tag{10}$$

Thus, the average power radiated by this dipole is given by the relation

$$P_{\rm rad}^{DPS} = \eta\frac{\pi}{3}\left|\frac{I_0 \ell}{\lambda}\right|^2 = 40\,(ka)^2\,|I_0|^2. \tag{11}$$

Electrically small dipole antennas in free space are inefficient radiators; the radiated power decreases quadratically as the size of the dipole relative to the wavelength decreases, i.e., as $(ka)^2$.

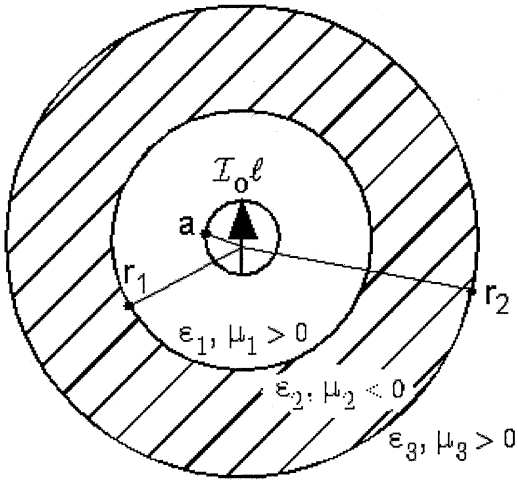

Fig. 1. Infinitesimal electric dipole of strength $I_0 l$ surrounded by a shell of DNG material with inner radius r_1 and outer radius r_2.

Similarly, the normalized reactance (4) measured at S is then given by the expression

$$X_R^{\rm DPS}(a) = -\frac{1}{(ka)^3}. \tag{12}$$

Electrically small dipole antennas have large capacitive reactances; the magnitude of the reactance ratio increases cubically as the size of the dipole relative to the wavelength decreases i.e., as $(ka)^{-3}$.

For a DNG medium, (5)–(9) are transformed by the substitutions $\varepsilon_{\rm real} \rightarrow -|\varepsilon_{\rm real}|$ and $\mu_{\rm real} \rightarrow -|\mu_{\rm real}|$. Investigators have also shown that the square root choices leading to $k_{\rm real} \rightarrow -|k_{\rm real}|$ and $\eta_{\rm real} \rightarrow +|\eta_{\rm real}|$ are required for DNG media [3]. For the case of an infinitesimal electric dipole immersed in a lossless DNG medium, one finds that the substitution $k \rightarrow -|k|$ in the dipole field formulas (5)–(9) holds even for the exponential terms, resulting in terms of the type $e^{+j|k|r}$. The radial power through the sphere of radius a for this case becomes

$$P_{\rm DNG} = \eta\frac{\pi}{3}\left|\frac{I_0 l}{\lambda}\right|^2\left[1 + \frac{j}{|ka|^3}\right] = P_{\rm DPS}^*. \tag{13}$$

The real component of the radial power is again positive, as expected from causality, while the reactive component is now positive, or inductive, rather than capacitive as it is in a DPS medium, i.e.,

$$P_{\rm rad}^{\rm DNG} = P_{\rm rad}^{\rm DPS}$$
$$X_R^{\rm DNG} = -X_R^{\rm DPS}. \tag{14}$$

This property led us to investigate whether the capacitive effect associated with an infinitesimal electric dipole in free space could be matched by an inductive effect associated with a DNG shell surrounding it.

III. Analytical Solution – Infinitesimal Dipole Surrounded by a DNG Shell

The configuration used in this study is shown in Fig. 1. An infinitesimal electric dipole of strength $I_0 l$ is located in a DPS

medium (Region 1) that is surrounded by a shell of DNG material (Region 2) with inner radius r_1 and outer radius r_2. The DPS medium outside of the DNG shell (Region 3) extends to infinity in all directions. The electric and magnetic fields for this configuration are given as follows:

Region 1

$$H_\phi^1 = \frac{jk_1 Il\sin\theta}{4\pi r}\left[1+\frac{1}{jk_1 r}\right]e^{-jk_1 r}+C_1\sin\theta j_1(k_1 r) \quad (15)$$

$$E_\theta^1 = \frac{j\eta_1 k_1 Il\sin\theta}{4\pi r}\left[1+\frac{1}{jk_1 r}-\frac{1}{(k_1 r)^2}\right]e^{-jk_1 r} - \frac{C_1\sin\theta}{j\omega\varepsilon_1 r}\left[(k_1 r)j_1'(k_1 r)+j_1(k_1 r)\right] \quad (16)$$

$$E_r^1 = \frac{\eta_1 Il\cos\theta}{2\pi r^2}\left[1+\frac{1}{jk_1 r}\right]e^{-jk_1 r}+\frac{2C_1\cos\theta}{j\omega\varepsilon_1 r}j_1(k_1 r). \quad (17)$$

Region 2

$$H_\phi^2 = C_2\sin\theta\left[j_1(k_2 r)+C_3 n_1(k_2 r)\right] \quad (18)$$

$$E_\theta^2 = \frac{-C_2\sin\theta}{j\omega\varepsilon_2 r}\left\{k_2 r\left[j_1'(k_2 r)+C_3 n_1'(k_2 r)\right] + j_1(k_2 r)+C_3 n_1(k_2 r)\right\} \quad (19)$$

$$E_r^2 = \frac{C_2 2\cos\theta}{j\omega\varepsilon_2 r}\left[j_1(k_2 r)+C_3 n_1(k_2 r)\right]. \quad (20)$$

Region 3

$$H_\phi^3 = C_4\sin\theta\, h_1^{(2)}(k_3 r) \quad (21)$$

$$E_\theta = \frac{-C_4\sin\theta}{j\omega\varepsilon_3 r}\left[(k_3 r)\, h_1^{(2)\prime}(k_3 r)+h_1^{(2)}(k_3 r)\right] \quad (22)$$

$$E_r = \frac{C_4 2\cos\theta}{j\omega\varepsilon_3 r}h_1^{(2)}(k_3 r) \quad (23)$$

where $j_1(kr)$ and $n_1(kr)$ represent the first order spherical Bessel functions of the first and second kind, respectively, $h_1^{(2)}(kr)$ represents the first order spherical Hankel function of the second kind, and all derivatives are to be taken with respect to the function's argument. The coefficients C_1-C_4 are found by imposing the electromagnetic boundary conditions, that E_θ and H_ϕ must be continuous across the material interfaces at radii r_1 and r_2. The coefficients then take the form:

$$C_1 = \frac{X_4 X_3 - \varepsilon_2 X_2}{\frac{\varepsilon_2}{\varepsilon_1}\left[(k_1 r_1)j_1'(k_1 r_1)+j_1(k_1 r_1)\right] - X_4 j_1(k_1 r_1)} \quad (24)$$

$$C_2 = \frac{X_3 + C_1 j_1(k_1 r_1)}{j_1(k_2 r_1)+C_3 n_1(k_2 r_1)} \quad (25)$$

$$C_3 = \frac{-(k_2 r_2)j_1'(k_2 r_2)+(X_1-1)j_1(k_2 r_2)}{(k_2 r_2)n_1'(k_2 r_2)-(X_1-1)n_1(k_2 r_2)} \quad (26)$$

$$C_4 = \frac{C_2\left[j_1(k_2 r_2)+C_3(k_2 r_2)\right]}{h_1^{(2)}(k_3 r_2)} \quad (27)$$

where

$$X_1 = \frac{\varepsilon_2}{\varepsilon_3}\left(1+\frac{(k_3 r_2)h_1^{(2)\prime}(k_3 r_2)}{h_1^{(2)}(k_3 r_2)}\right) \quad (28)$$

$$X_2 = \frac{\omega\eta_1 k_1 I_0 l}{4\pi}\left[1+\frac{1}{jk_1 r_1}-\frac{1}{(k_1 r_1)^2}\right]e^{-jk_1 r_1} \quad (29)$$

$$X_3 = \frac{jk_1 I_0 l}{4\pi r_1}\left[1+\frac{1}{jk_1 r_1}\right]e^{-jk_1 r_1} \quad (30)$$

$$X_4 = 1+\frac{k_2 r_1\left[j_1'(k_2 r_1)+C_3 n_1'(k_2 r_1)\right]}{j_1(k_2 r_1)+C_3 n_1(k_2 r_1)}. \quad (31)$$

IV. Numerical Results for DNG Medium Dual to Free Space

The real power radiated by an infinitesimal electric dipole surrounded by a shell of DNG material and the normalized reactance of the dipole antenna were analyzed numerically using (1), (15)–(31). Analytic continuation was utilized to calculate the requisite spherical Bessel, Neumann, and Hankel functions with negative arguments [12]. The validity of these equations and the accuracy of their MATLAB software implementation were tested by comparing the software's output to known analytical results, particularly for the case where all regions contained free space, that is, for $(\varepsilon_1,\mu_1)=(\varepsilon_2,\mu_2)=(\varepsilon_3,\mu_3)=(\varepsilon_0,\mu_0)$. The case of a DNG shell whose properties are "dual" to those of free space was first analyzed using the following parameters: $(\varepsilon_1,\mu_1)=(\varepsilon_3,\mu_3)=(\varepsilon_0,\mu_0)$, $(\varepsilon_2,\mu_2)=(-\varepsilon_0,-\mu_0)$, $f=10\,\mathrm{GHz}=c/\lambda_0$, and $I_0 l=2\lambda_0/1000\,\mathrm{A\cdot m}$ with $I_0=1\,\mathrm{A}$. For simplicity, the permittivity and permeability values were chosen to achieve matched media across the boundaries at r_1 and r_2, i.e., to have $\eta_1=\eta_2=\eta_3$ with $\eta_j=\sqrt{\mu_j/\varepsilon_j}$. These material parameters made comparisons to the free space case easier; and since each region is matched, any disruption in the formation of the dipole field would be mainly caused by changes in the wave physics inside the DNG shell, rather than by interface scattering effects. The frequency ($f=10\,\mathrm{GHz}$) and the initial choice of the inner radius of the DNG shell ($r_1=100\,\mu\mathrm{m}=\lambda_0/300\sim 4\,\mathrm{mils}$) were chosen according to experimental efforts associated with current metamaterial research.

A plot of the radiated power gain of the dipole-DNG shell system (radiated power in the DNG case normalized to the corresponding free space, DPS value)

$$P_{\mathrm{gain}} = \frac{P_{\mathrm{rad,DNG}}}{P_{\mathrm{rad,DPS}}} \quad (32)$$

versus the outer DNG shell radius is given in Fig. 2(a) for values $r_2\geq r_1=100\,\mu\mathrm{m}=0.1$ mm. The effective radius of the infinitesimal electric dipole was $a=\lambda_0/1000$. The value of the outer radius that maximized the real power radiated by the dipole was found to be $r_2=748.8\,\mu\mathrm{m}=.025\lambda_0$, hence, $kr_2=0.157$, which is small but larger than $ka=2\pi/1000=0.006\,28$. This maximum value was $P_{\mathrm{rad,DNG}}=1.162\times 10^{-1}$ W. As seen in Fig. 2(a), a significant improvement in the radiated power could still be obtained for a much smaller DNG shell size. For example, 80% of the maximum possible radiated power could be obtained for $r_2=364\,\mu\mathrm{m}=.012\lambda_0$, which is less than half of the optimum outer radius and gives $kr_2=0.0785$. The normalized reactance was calculated for all cases as indicated in Section II. A plot of the reactance ratio

$$X_{\mathrm{Ratio}}(a) = \frac{\left|X_R^{DNG}(a)\right|}{\left|X_R^{DPS}(a)\right|} \quad (33)$$

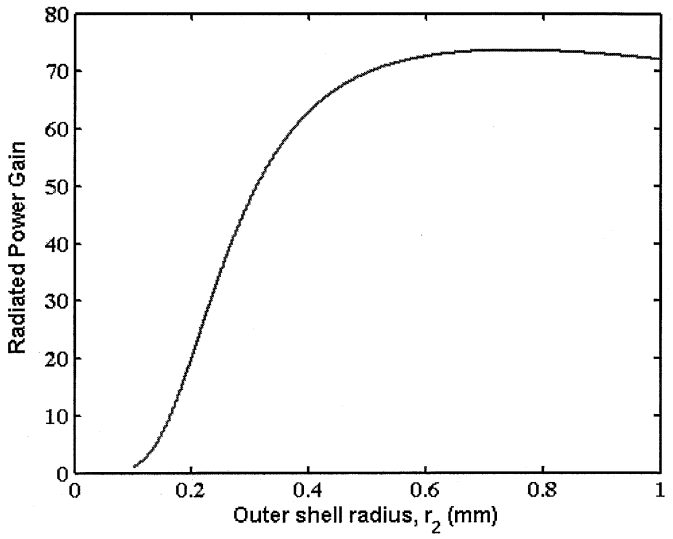

(a)

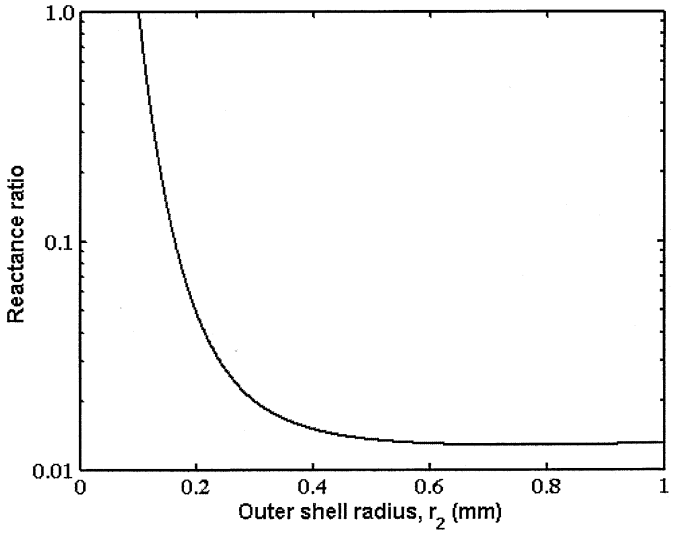

(b)

Fig. 2. (a) Radiated power gain and (b) reactance ratio of an infinitesimal electric dipole surrounded by a DNG shell with inner radius $r_1 = 100\ \mu\mathrm{m}$ and variable outer radius r_2. The maximum radiated power is produced when $r_2 = 748.8\ \mu\mathrm{m}$, but 80% of this maximum may be obtained when the outer radius is just 364 $\mu\mathrm{m}$.

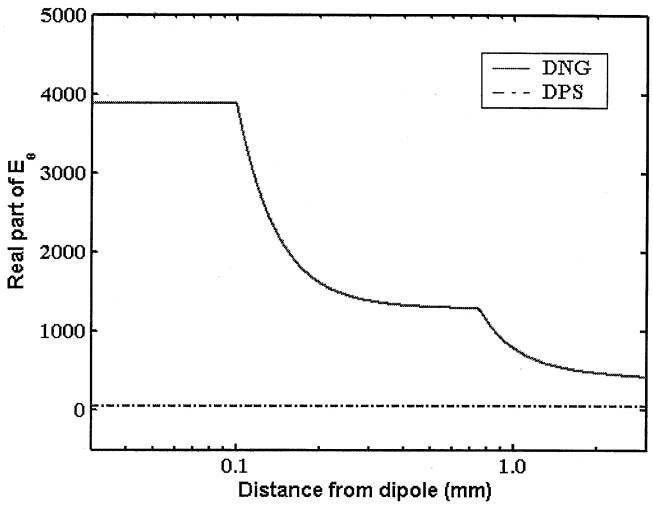

(a)

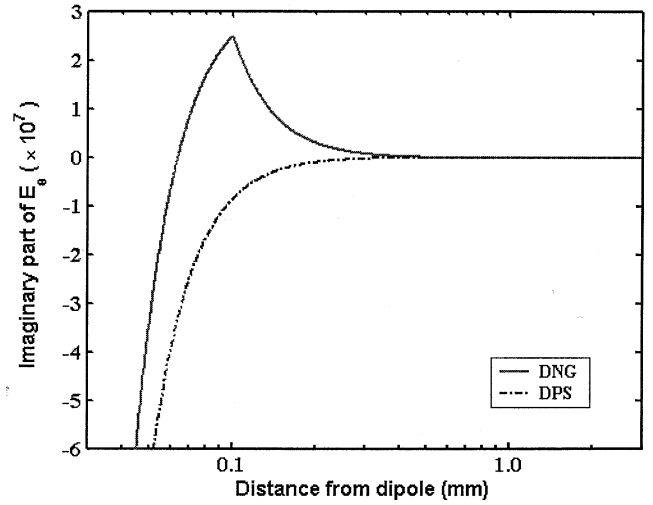

(b)

Fig. 3. (a) Real and (b) imaginary components of E_θ are shown as functions of the distance from the infinitesimal electric dipole for the DNG and DPS (free space) cases. The DNG case has the DNG shell placed between a radius of 100 and 748.8 $\mu\mathrm{m}$. Note that E_θ is continuous across boundaries, as expected, but its derivative is discontinuous due to the changing signs of ε and μ. Also note that, in some areas, the reactive component of E_θ for the DNG case is positive and of opposite sign to that of the free space case.

versus the outer DNG shell radius is given in Fig. 2(b). The value of the outer radius that minimized $X_R(a)$ was slightly different ($r_2 = 754.6\ \mu$m) from where the radiated power achieved its maximum, but the variance of $X_R(a)$ between the two r_2 values was 0.002%.

Figs. 3 and 4 compare the electric and magnetic fields generated in this DNG case with those produced when no DNG shell is present, i.e., with those for the dual DPS case. Note that while E_θ and H_ϕ are continuous at r_1 and r_2 by definition, their derivatives are discontinuous at the edges of the DNG shell due to the sign changes in ε and μ. Also note that, in this small region very near the antenna, the real part of E_θ for both the DPS and DNG medium cases is practically constant, while the imaginary component is changing by orders of magnitude. Moreover, note that unlike the DPS case the imaginary parts of both field components in the DNG case have significant swings between positive and negative values.

Fig. 5 compares the real and imaginary components of the Poynting's vector, in particular, the radiated real power $P_{\mathrm{rad}}(r)$ and the normalized reactance $X_R(r)$, for the DNG shell and the dual free space DPS configurations as a function of the distance from the dipole when the DNG shell radii are fixed at $r_1 = 100\ \mu\mathrm{m}$ and $r_2 = 748.8\ \mu\mathrm{m}$. When the DPS case is considered, these results are identical to their well-known values. To emphasize this fact in the DPS case and the increase or decrease in the DNG case, the radiated power gain values and reactance ratio values for both the DNG and the DPS configurations are given in Fig. 5(a) and (b). Note that the radiated power is independent of the radius, i.e., the radiated power gain stays constant at any radius. The non-normalized values are $P_{\mathrm{rad,DNG}} = 1.162 \times 10^{-1}$ W and $P_{\mathrm{rad,DPS}} = 1.578 \times 10^{-3}$ W. When the DNG shell is present, the real power radiated is thus 73.66 times greater than the free space result. Similarly, the normalized reac-

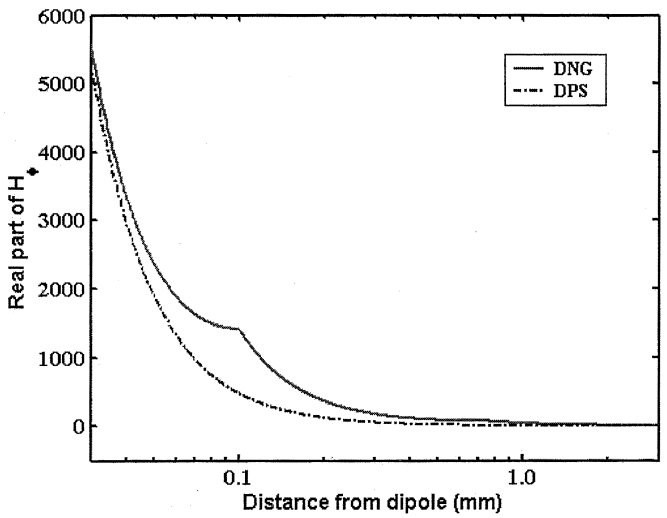

(a)

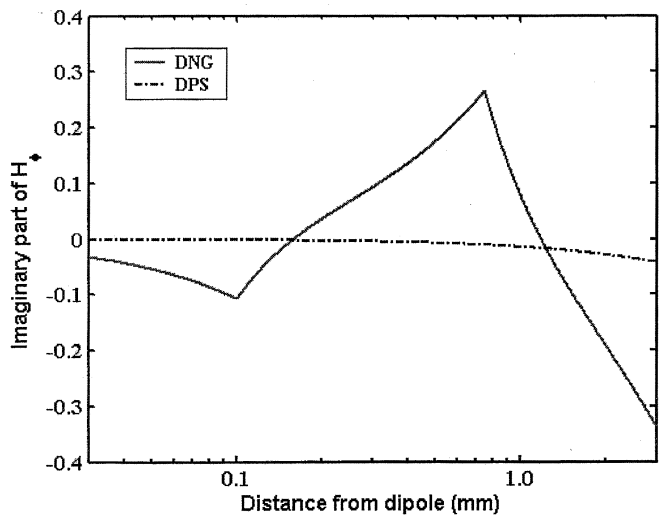

(b)

Fig. 4. (a) Real and (b) imaginary components of H_ϕ are shown as functions of the distance from the infinitesimal electric dipole for the DNG and DPS (free space) cases. The DNG case has the DNG shell placed between a radius of 100 and 748.8 μm. Note that H_ϕ is continuous across boundaries, but its derivative is discontinuous due to the changing signs of ε and μ.

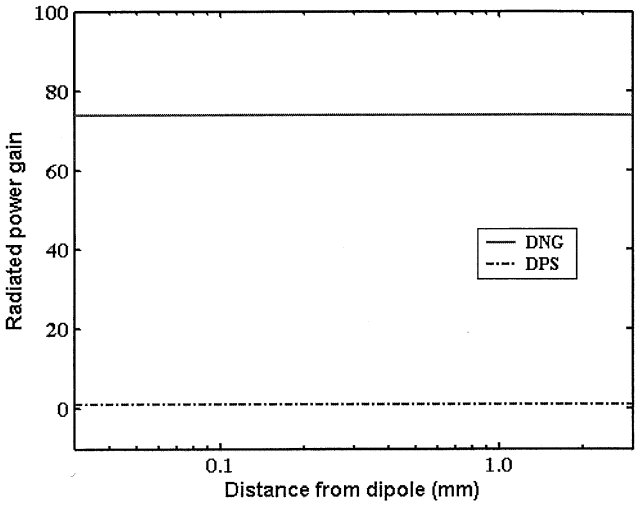

(a)

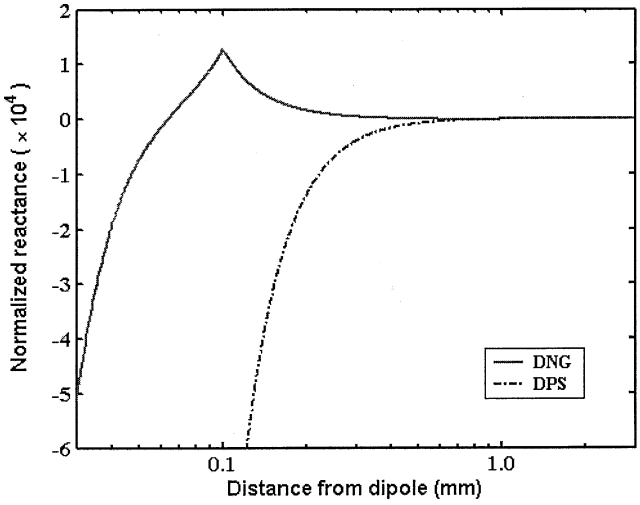

(b)

Fig. 5. (a) Radiated power gain and (b) the normalized reactance are shown as functions of the distance from the infinitesimal electric dipole for the DNG and DPS (free space) cases. The DNG case has the DNG shell placed between a radius of 100 and 748.8 μm.

tance values were calculated to be: $X_{R,DPS}(a) = 4.031 \times 10^6$ and $X_{R,DNG}(a) = 5.154 \times 10^4$. The DNG value $X_{R,DNG}(a)$ is 78.21 times smaller than the DPS value $X_{R,DPS}(a)$; this agrees very well with the noted gain in the radiated power.

The very good correlation between the normalized reactance decrease and the radiated power increase provides additional credence to the observed result: the dipole-DNG shell configuration outperforms the standard free-space dipole. We note that the radiated power increase predicted by (11) simply due to an increase in the dipole length from a to r_2 is only $(r_2/a)^2 = 11.11$; the DNG shell result is substantially larger. We note that Fig. 5(b) clearly shows, as anticipated, that the reactive power component of the DNG case is opposite in sign to the free space case in some areas. This means that the DNG shell does indeed serve to partially "match" the antenna to free space, and this matching leads to the observed enhanced performance of the dipole-DNG shell system. Thus the reduced reactance results in Fig. 2(b) can be interpreted to mean that if $r_1 = 100\ \mu$m, the DNG shell with $r_2 = 748.8\ \mu$m provides the best "matching network" between the dipole and free space.

V. Lumped Element Model

Because the dipole antenna-DNG shell system model predicts unusual behavior, a lumped element circuit model similar to the free-space one introduced by Chu [13] and Harrington [5] is presented to augment the exact analysis above. This circuit approach has been used again recently by Grimes and Grimes [14] to argue a violation of the Chu-Harrington limit and by Collin [15] to re-examine their conclusions. The development of such a lumped parameter model in the present case would help ascertain the validity of the analytical results.

Reconsider the geometry shown in Fig. 1. As discussed in Harrington [5], an electric dipole radiating a TM_{10} mode into free space can be represented by a high-pass circuit. The spatial cutoff associated with this circuit provides an explanation for

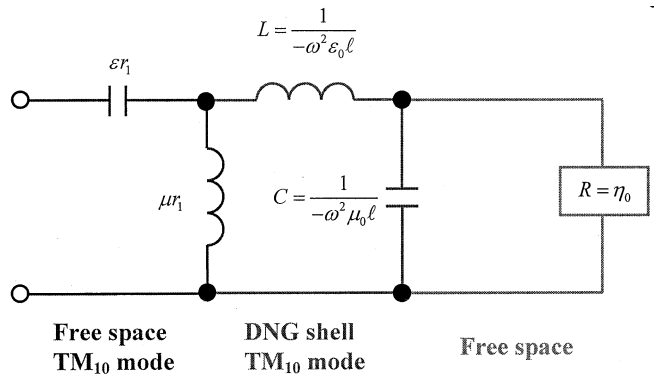

Fig. 6. Lumped element circuit for an electrically small dipole antenna radiating a TM_{10} mode into a free space sphere of radius r_1 that is surrounded by a spherical shell of DNG material having a thickness ℓ and is terminated with a free space region.

the high reactance and corresponding high radiation Q when the dipole antenna is electrically small. For the DNG shell case, we assume that the dipole is radiating into a free space sphere of radius r_1. This representation is the first section of the circuit diagram shown in Fig. 6. The circuit representation for the surrounding DNG shell is the second section shown in Fig. 6; its values of the capacitance and inductance were obtained using the results given by Iyer and Eleftheriades in [16]. For simplicity of the discussion, it is here assumed that the DNG medium has $\varepsilon = -\varepsilon_0$ and $\mu = -\mu_0$ and has a thickness $\ell = r_2 - r_1$. As suggested by Ramo *et al.* [8, pp. 257–258], such a backward-wave medium representation can be obtained from the dual of the DPS case, as it is deduced here. The transmission line is terminated with free space, whose impedance is $R = \eta_0$, as shown by the last section in Fig. 6.

The input impedance, Z_{in}, of this circuit is obtained straightforwardly. One finds that (see (34) at the bottom of the page). With $k_0^2 = \omega^2 \varepsilon_0 \mu_0$ and the values for the capacitance and inductance of the DNG medium circuit, this can be rewritten in the form (see (35) at the bottom of the page). To achieve the desired lowering of the normalized reactance, one would desire to have the imaginary part of the complex power, hence, of the input impedance vanish. This would mean that there would be no reactance associated with the entire radiation process. Consider then a simple case with $\ell \simeq r_1$. The imaginary term in the braces in the numerator of (35) becomes $1 - 4(k_0\ell)^2 + 4(k_0\ell)^4$. This is identically zero for $(k_0\ell)^2 = 1/2$, i.e., for $\ell = \lambda/(2\sqrt{2}\pi)$. In fact, one then finds in this case that $Z_{\mathrm{in}} \equiv R$. The presence of the DNG medium has taken the radiation process from below cutoff to a perfect match to free space. This correlates with the observed transformation above of the reactive power to radiated power, and the corresponding decrease in the reactance when the parameters of the DNG shell have been optimized.

A comparison of the values of the circuit model Z_{in} predicted by (35) for this test case and those obtained from the analytical field model further demonstrate a reasonable correspondence between these two models. The real and imaginary components of the input impedance Z_{in} normalized by the free space impedance η_0 for $r_1 = \lambda_0/(2\sqrt{2}\pi) = 3.376$ mm are shown, respectively, in Fig. 7(a) and (b) as a function of the outer radius of the DNG shell r_2. The real part goes through one and the imaginary part goes through zero when $r_2 = 2r_1 = 6.752$ mm as predicted. On the other hand, the radiated power gain normalized to its maximum value, 5.70, for the same case is also given in Fig. 7(a). It achieves its maximum at the nearby outer radius value $r_2 = 7.8\ \mathrm{mm}$. Both curves in Fig. 7(a) show the existence of an optimum value. While the circuit model and its corresponding results are approximate, because the complete propagation effects of the transmission lines have not been included in this analysis as they were in the analytical dipole results, it nonetheless reveals that the DNG shell could indeed be used as an impedance matching network for the electrically-small electric dipole antenna radiating into free space with the result that there is a gain in the radiated real power. It thus lends further credence to the analytical and the corresponding numerical results given above and below.

VI. Numerical Results for General DNG Media

While the initial choice for the matched DNG medium, $(\varepsilon_{2r}, \mu_{2r}) = (-1, -1)$, was made because of its immediate connection to the free space DPS case with $(\varepsilon_{jr}, \mu_{jr}) = (+1, +1)$ for $j = 1, 2, 3$, additional DNG media were explored to investigate the impact of various parameters on gain enhancement and reactance reduction. In particular, it was found that the power radiated by (reactance of) the dipole could be increased (decreased) when the permittivity and permeability of the DNG shell were decreased (i.e., made more negative). Similar radiated power increases (reactance decreases) were also found by decreasing the inner radius r_1 of the DNG shell. Both variations provided stronger interactions between the radiating

$$Z_{\mathrm{in}} = R\frac{1 - \omega^2(L + \mu_0 r_1)C - \omega^2 \varepsilon_0 \mu_0 r_1^2(1 - \omega^2 LC) + j\omega[\mu_0 r_1 + L(1 - \omega^2 \varepsilon_0 \mu_0 r_1^2)]}{j\omega\varepsilon_0 r_1[R + j\omega(L + \mu_0 r_1) - \omega^2 RC(L + \mu_0 r_1)]}. \tag{34}$$

$$Z_{\mathrm{in}} = R\frac{(k_0 r_1)^4 (k_0\ell)^4 - jk_0 r_1\{1 - (k_0\ell)^2\left(1 + \frac{r_1}{\ell}\right)^2 + (k_0\ell)^4[1 + 2\left(\frac{r_1}{l}\right)^2 + \left(\frac{r_1}{\ell}\right)^3]\}}{(k_0 r_1)^2\{1 - (k_0\ell)^2[1 + 2\left(\frac{r_1}{\ell}\right)] + (k_0\ell)^4[1 + \left(\frac{r_1}{\ell}\right)^2] + (k_0 r_1)^2(k_0\ell)^4\}}. \tag{35}$$

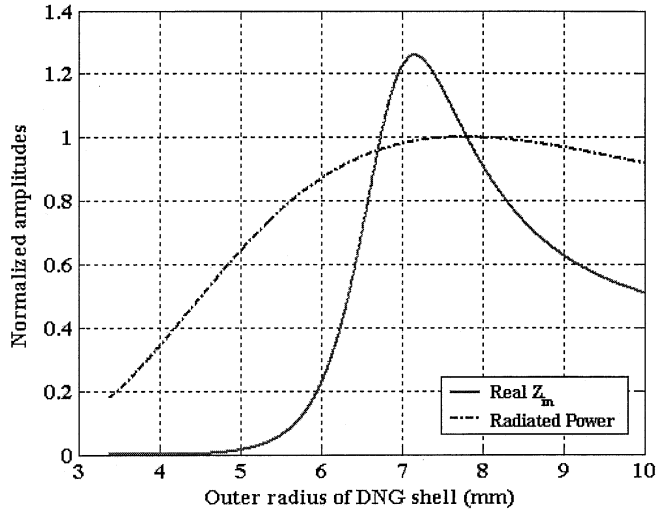

(a)

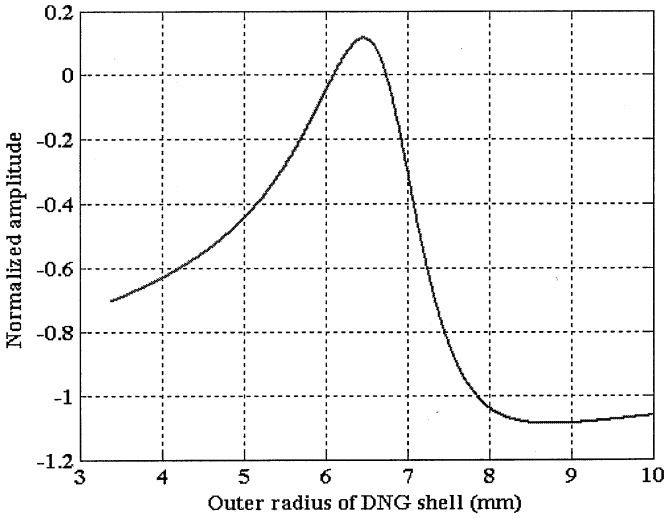

(b)

Fig. 7. Circuit model input impedance variation with the outer radius r_2 of the DNG shell: (a) real part and (b) imaginary part, normalized to the free space value η_0. The reactive (imaginary) part passes through a null as the normalized real part passes through one.

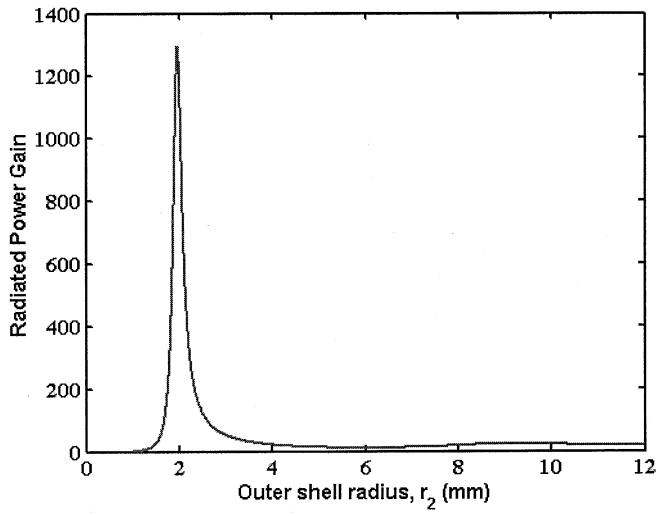

(a)

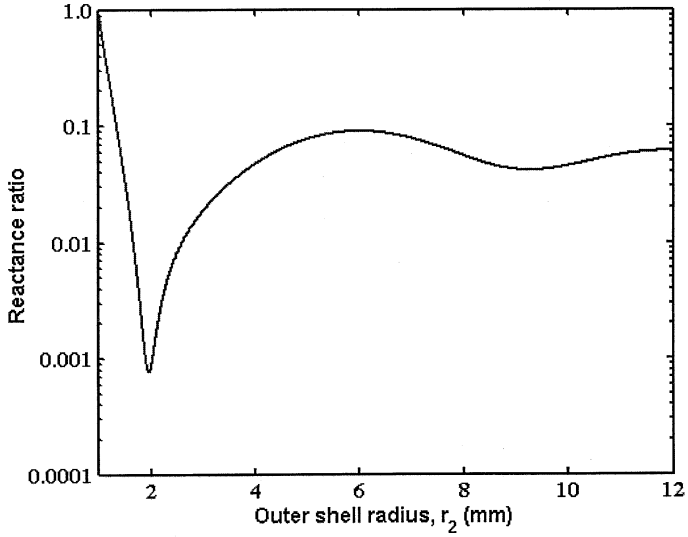

(b)

Fig. 8. (a) Radiated power and (b) reactance ratio of an infinitesimal electric dipole surrounded by a DNG shell with inner radius $r_1 = 1.0\ \mathrm{mm}$ and variable outer radius r_2. The dipole radiated at 10 GHz, and the DNG shell had the parameters $(\varepsilon_2, \mu_2) = (-3\varepsilon_0, -3\mu_0)$. One strong and a few weaker resonant shell sizes are observed. The first two resonances are explored in Figs. 9–10.

dipole and the DNG shell, hence, more complete matching between them.

To illustrate these points, Figs. 8–10 show sample results for the radiated power gain P_{gain} and the reactance ratio X_{ratio} achieved by a DNG shell with $(\varepsilon_2, \mu_2) = (-3\varepsilon_0, -3\mu_0)$ and inner radius $r_1 = 1.0$ mm. The frequency was again set to 10 GHz ($\lambda_0 = 3.0$ cm). Fig. 8 shows the radiated power gain and reactance ratio as functions of the outer radius r_2 of the DNG shell. When the shell's outer radius approaches 1.9661 mm ($r_2 \sim \lambda_0/15$), a strong resonance is seen to occur; the power radiated is 1.298×10^3 times that radiated by the dipole into free space alone. The normalized reactance simultaneously is 1.298×10^3 times smaller than the free space value. Another resonance is seen near an outer radius of 9.27 mm ($r_2 \sim \lambda_0/3$). Although this resonance is weaker than the first, it is also appreciably broader, and it still produces 24.2 times the power radiated by the dipole into free space. The behaviors of the radiated power gain and reactance ratio near these individual resonances are shown, respectively, in Figs. 9 and 10. The actual values of $X_{R,\,DNG}(a)$ at these two maxima are 3.107×10^3 and 1.666×10^5, respectively.

If the inner radius of the DNG shell is reduced still further, or if the permittivity and permeability of the DNG medium are decreased even more, the resonances become narrower and more pronounced. An example for the case when $(\varepsilon_2, \mu_2) = (-3\varepsilon_0, -3\mu_0)$ and $r_1 = 100\ \mu$m is shown in Fig. 11. The radiated power gain is given in Fig. 11(a); the corresponding reactance ratio values are given in Fig. 11(b). This case produces a spectacular $1.6532 \times 10^9 = 92.18\ \mathrm{dB}$ radiated power gain for $r_2 = 185.8004\ \mu\mathrm{m} \sim \lambda_0/161$. The reactance ratio drops to the value $2.2606 \times 10^{-5} = -46.46\ \mathrm{dB}$ where the gain peak occurs but has a nearby minimum of $3.9302 \times 10^{-9} = -84.06\ \mathrm{dB}$ at the nearby value $r_2 = 184.6893\ \mu\mathrm{m}$. Note that the width of the resonance is extremely narrow, corresponding to a DNG shell

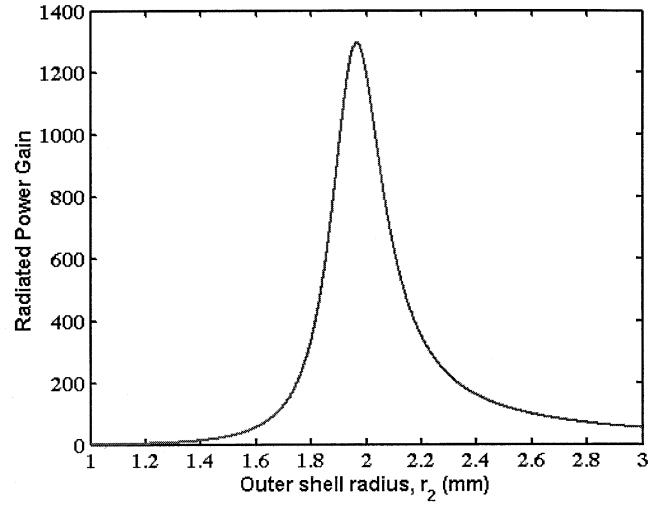

(a)

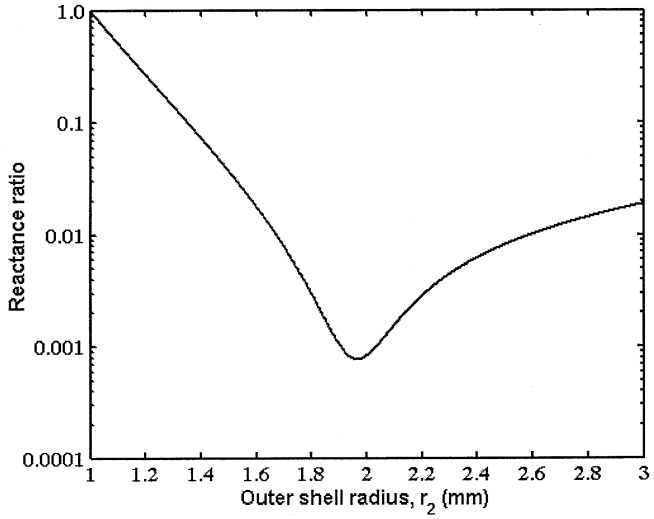

(b)

Fig. 9. (a) Radiated power gain and (b) reactance ratio for the first resonant peak seen in Fig. 8. When the outer radius of the DNG shell approaches 1.9661 mm, the radiated power gain peaks at 1298 while the reactance ratio drops to 7.704×10^{-2}.

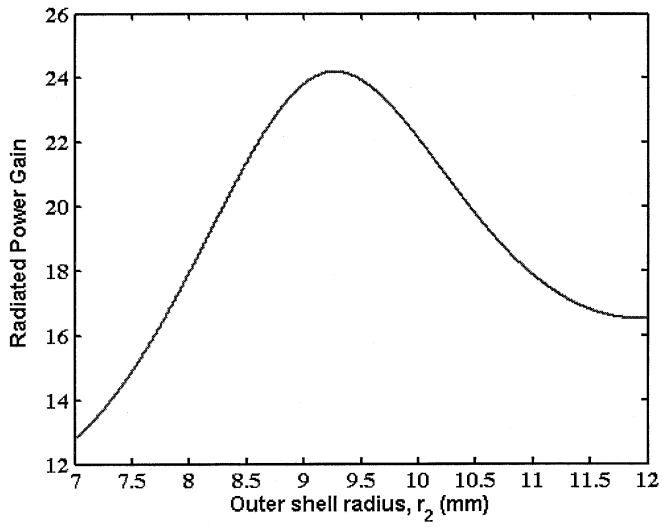

(a)

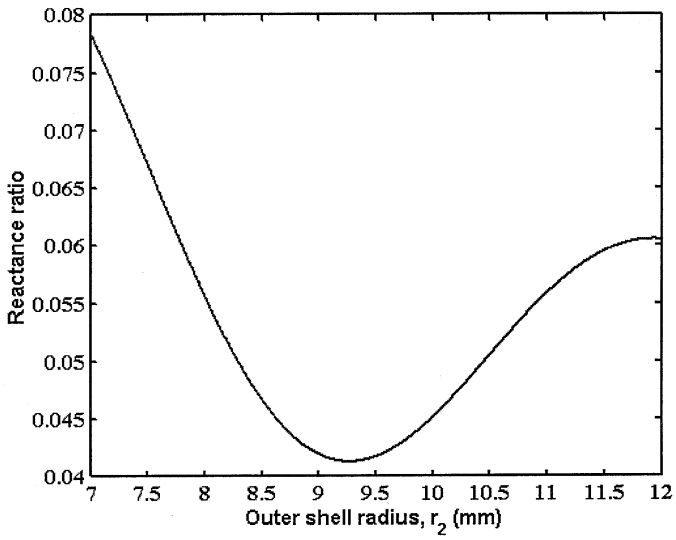

(b)

Fig. 10. (a) Radiated power gain and (b) reactance ratio for the second resonant peak seen in Fig. 8. When the outer radius of the DNG shell approaches 9.27 mm, the radiated power gain peaks at 24.2 while the reactance ratio drops to 4.13×10^{-2}.

for which the allowed variation in r_2 is extremely small. Moreover, the DNG shell itself is very thin. Thus, it may be a difficult case to realize physically with many of the current metamaterial realizations of DNG media. On the other hand, note that there are larger radii DNG shells that produce less, but still very significant radiated power gains. This is verified with the plot of the radiated power gain of the dipole-DNG shell system as a function of the inner radius r_1 with the outer radius optimized shown in Fig. 12. Finally, note that the value of $X_{R,\,DNG}(a)$ when $r_2 = 185.8004\ \mu$m is $+91.13$ which shows that the dipole-DNG shell system is slightly inductive in contrast to the DPS value -4.0313×10^6 which corresponds to the very capacitive dipole interaction with free space.

To demonstrate the behavior of the DNG shell configurations as the material parameters vary, a lossless Drude medium model of the DNG medium was introduced, i.e., the relative permittivity and permeability was set to the frequency dependent form

$$\varepsilon_{2r} = \frac{\varepsilon_2}{\varepsilon_0} = \mu_{2r} = \frac{\mu}{\mu_0} = 1 - \frac{\omega_p^2}{\omega^2}. \tag{36}$$

The plasma frequency was set to $f_p = 20$ GHz so that at $f = 10$ GHz one has $\varepsilon_r = \mu_r = -3.0$. At frequencies below 10 GHz the DNG medium was more negative; it was less negative for frequencies between 10 and 20 GHz . The radiated power gain and the reactance ratio for the DNG shell with $r_1 = 1.0$ mm and $r_2 = 1.9661$ mm are shown in Fig. 13, and they are shown in Fig. 14 for $r_1 = 100\ \mu$m and $r_2 = 185.8004\ \mu$m. To obtain Fig. 13, 18 000 samples were taken in the frequency band 1–19 GHz . To obtain Fig. 14, 110 000 samples were taken in the frequency band 8–19 GHz . Clearly, additional highly resonant frequencies were uncovered for both more and less negative DNG media for a fixed shell size.

We also note that because all of the dipole-DNG shell system formulas depend explicitly on products of a wavenumber and a sphere radius, the results for DNG shells of varying thickness at a fixed frequency are related immediately to results for a fixed DNG shell thickness and varying frequency. Thus, all of the

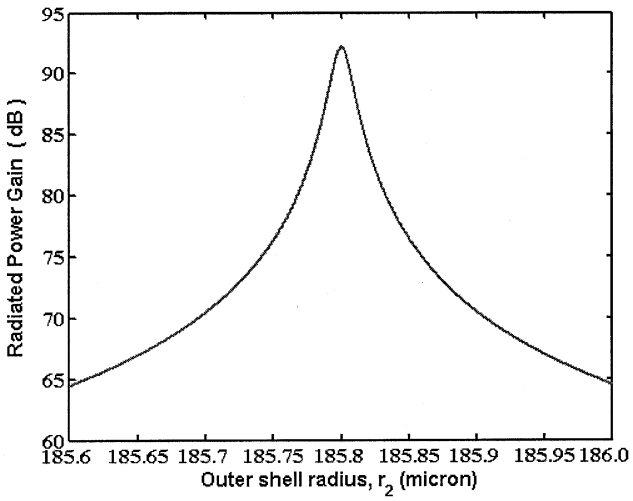

(a)

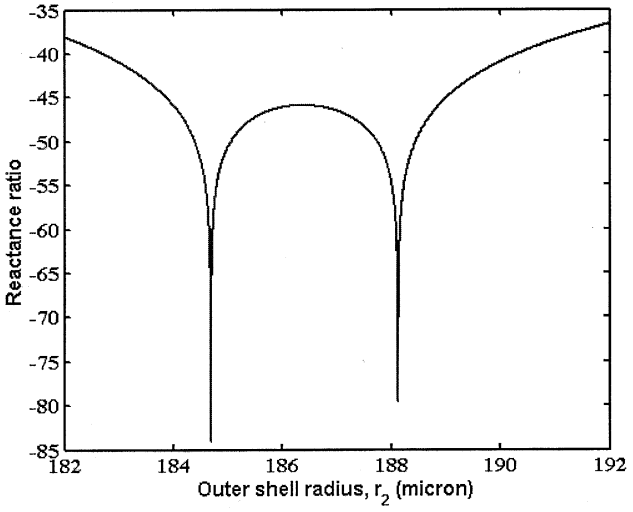

(b)

Fig. 11. (a) Radiated power gain and (b) reactance ratio of an infinitesimal electric dipole surrounded by a DNG shell with a smaller inner radius of $r_1 = 100\ \mu$m and variable outer radius r_2. The dipole radiated at 10 GHz, and the DNG shell had the parameters $(\varepsilon_2, \mu_2) = (-3\varepsilon_0, -3\mu_0)$. The radiated power gain is seen to peak at a value of 1.6532×10^9 for $r_2 = 185.8004\ \mu$m $\sim \lambda_0/161$. The reactance ratio drops to the value $2.2606 \times 10^{-5} = -46.46$ dB where the gain peak occurs but has a nearby minimum of $3.9302 \times 10^{-9} = -84.06$ dB at $r_2 = 184.6893\ \mu$m.

results presented here are scalable to other frequency regimes and to other sizes of the dipole-DNG shell systems.

VII. Energy Calculation of the Reactance of the Dipole-DNG Shell System

The reactance of the dipole-DNG shell system may also be calculated using the average stored energies as indicated by (3). However, this calculation must proceed with some care. In particular, one observes immediately that the standard expressions, (3), for the average energies W_e and W_m stored in a volume V yield negative values in a DNG medium. Thus, if we follow Maxwell's equations with no intervention and allow these terms to be negative, their explicit interpretation as stored energy would be unorthodox.

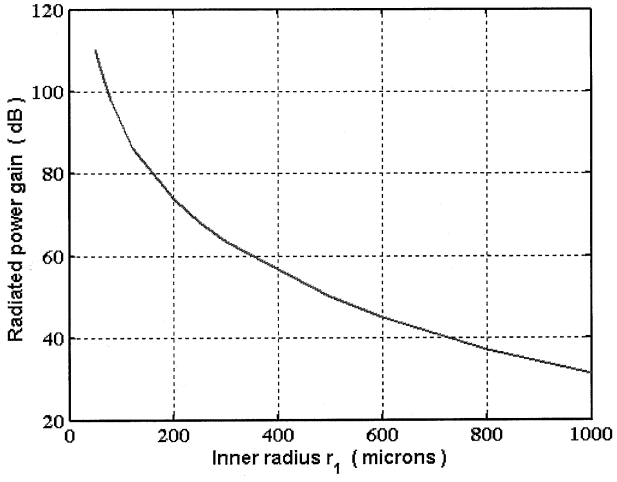

Fig. 12. Radiated power gain (dB) is shown as a function of the inner radii r_1 of the DNG shell with $(\varepsilon_2, \mu_2) = (-3\varepsilon_0, -3\mu_0)$. The outer radius r_2 of the DNG shell was selected to optimize this gain.

One would expect that the input reactance seen by the dipole would be measured at $r = a$. This is further confirmed in view of the circuit representation of the dipole-DNG shell system given in Fig. 6. In all the cases considered above, the normalized reactance $X_R(a)$ was calculated at $r = a$ using the real and imaginary parts of the complex Poynting's vector. Thus all of those results should be recovered if one uses (4) with the same $P_{\rm rad}$ values but now with the expression $P_{\rm reac} = 2\omega(W_m - W_e)$ given in (2). We claim that if the reactance is to be properly calculated in this manner using W_e and W_m, then the negative sign associated with the DNG medium must be present in the calculation of W_e and W_m.

To prove this, we expand (3) in terms of those calculations over each region of the dipole-DNG shell system. The electric and magnetic energy terms can then be written explicitly as

$$\begin{aligned} W_e(r_{\rm obs}) =& \frac{4\pi}{3}\int_a^{r_1} dr\, r^2 \left\{\frac{1}{2}\varepsilon_1 |e_r|^2 + \frac{1}{2}\varepsilon_1 |e_\theta|^2\right\} \\ &+ \frac{4\pi}{3}\int_{r_1}^{r_2} dr\, r^2 \left\{\frac{1}{2}\,\varepsilon_2\, |e_r|^2 + \frac{1}{2}\,\varepsilon_2\, |e_\theta|^2\right\} \\ &+ \frac{4\pi}{3}\int_{r_2}^{r_{\rm obs}} dr\, r^2 \left\{\frac{1}{2}\varepsilon_3 |e_r|^2 + \frac{1}{2}\varepsilon_3 |e_\theta|^2\right\} \\ W_m(r_{\rm obs}) =& \frac{4\pi}{3}\int_a^{r_1} dr\, r^2 \left\{\frac{1}{2}\mu_1 |h_\phi|^2\right\} \\ &+ \frac{4\pi}{3}\int_{r_1}^{r_2} dr\, r^2 \left\{\frac{1}{2}\mu_2\, |h_\phi|^2\right\} \\ &+ \frac{4\pi}{3}\int_{r_2}^{r_{\rm obs}} dr\, r^2 \left\{\frac{1}{2}\mu_3\, |h_\phi|^2\right\} \end{aligned} \tag{37}$$

where e_r, e_θ, h_ϕ are the portions of the time harmonic dipole fields that depend only on the radius r. In the limit $r_{\rm obs} \to \infty$, these terms recover those given by (3). In contrast, if one were to insist that only positive energies are to be allowed in this calculation, then, as a natural choice, one could introduce

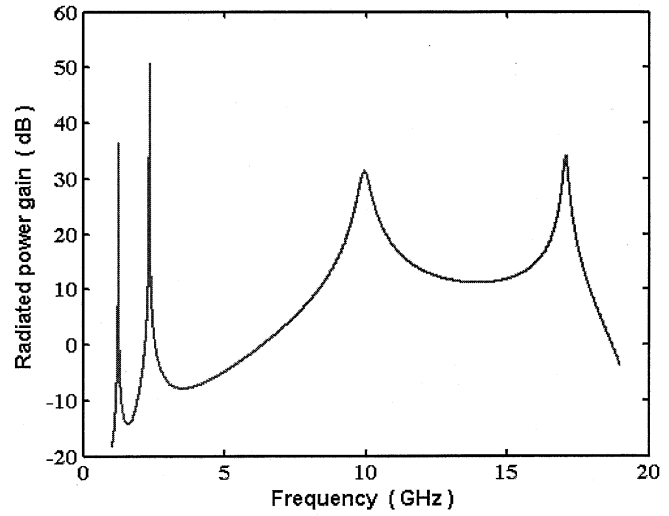

(a)

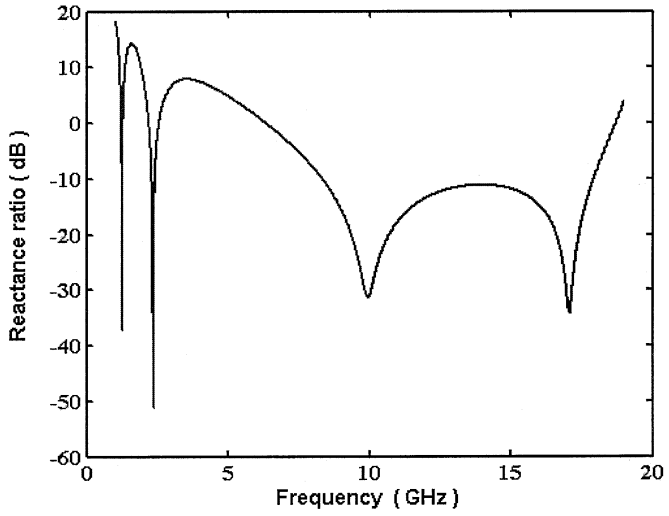

(b)

Fig. 13. (a) Radiated power gain and (b) the reactance ratio are shown as a function of the frequency for a Drude model DNG shell with $r_1 = 1.0$ mm and $r_2 = 1.9661$ mm. Several resonant radiated power gain peaks are present as the frequency and, hence, the DNG permittivity and permeability values vary.

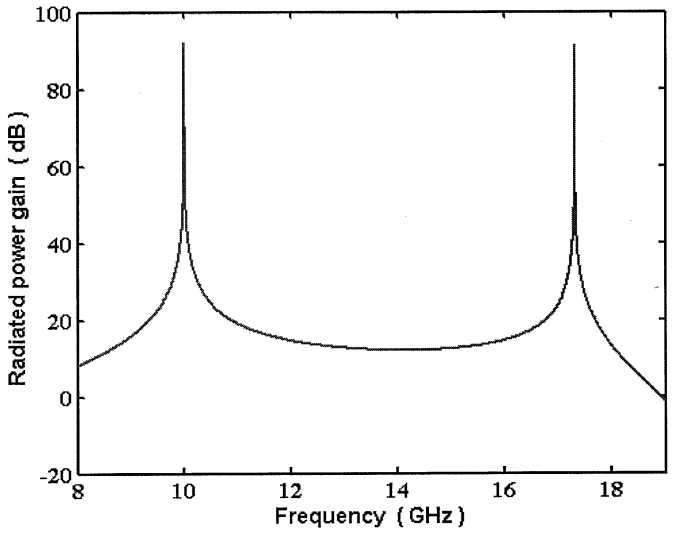

(a)

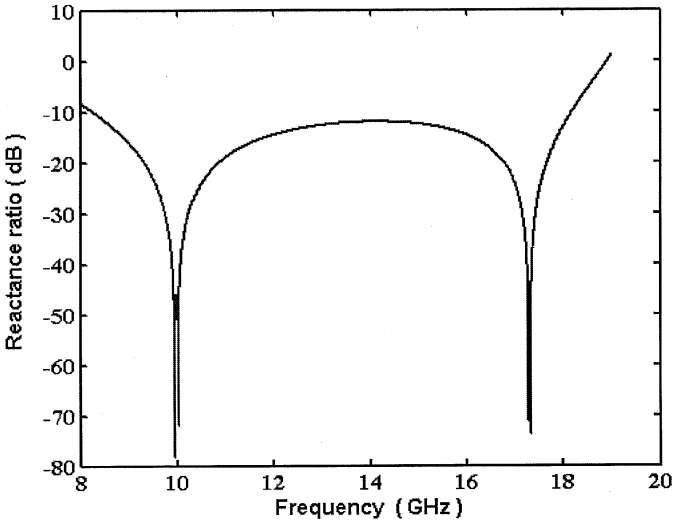

(b)

Fig. 14. (a) Radiated power gain and (b) the reactance ratio are shown as a function of the frequency for a Drude model DNG shell with $r_1 = 100\ \mu$m and $r_2 = 185.8004\ \mu$m. Several resonant radiated power gain peaks are present as the frequency and, hence, DNG permittivity and permeability values vary.

the absolute value signs into (37) to obtain the positive definite energy expressions

$$\begin{aligned} W_e^{\rm pos}(r_{\rm obs}) =& \frac{4\pi}{3}\int_a^{r_1} dr\, r^2 \left\{\frac{1}{2}\,|\varepsilon_1|\,|e_r|^2 + \frac{1}{2}\,|\varepsilon_1|\,|e_\theta|^2\right\} \\ &+ \frac{4\pi}{3}\int_{r_1}^{r_2} dr\, r^2 \left\{\frac{1}{2}\,|\varepsilon_2|\,|e_r|^2 + \frac{1}{2}\,|\varepsilon_2|\,|e_\theta|^2\right\} \\ &+ \frac{4\pi}{3}\int_{r_2}^{r_{\rm obs}} dr\, r^2 \left\{\frac{1}{2}\,|\varepsilon_3|\,|e_r|^2 + \frac{1}{2}\,|\varepsilon_3|\,|e_\theta|^2\right\} \\ W_m^{\rm pos}(r_{\rm obs}) =& \frac{4\pi}{3}\int_a^{r_1} dr\, r^2 \left\{\frac{1}{2}\,|\mu_1|\,|h_\phi|^2\right\} \\ &+ \frac{4\pi}{3}\int_{r_1}^{r_2} dr\, r^2 \left\{\frac{1}{2}\,|\mu_2|\,|h_\phi|^2\right\} \\ &+ \frac{4\pi}{3}\int_{r_2}^{r_{\rm obs}} dr\, r^2 \left\{\frac{1}{2}\,|\mu_3|\,|h_\phi|^2\right\} \end{aligned} \tag{38}$$

The reactance values obtained using (37) and (38) were analyzed for the highly resonant case with $(\varepsilon_2, \mu_2) = (-3\varepsilon_0, -3\mu_0)$, $r_1 = 100\ \mu$m and $r_2 = 185.8004\ \mu$m. The calculation of (37) and (38) was segmented into two regions to increase its accuracy, i.e., the integration was divided into 30 000 intervals between a and $2r_2$ and 30 000 intervals between $2r_2$ and $r_{\rm obs} = 10.0$ mm. The smaller Δr in the first region allowed better resolution of the large variations in the field values at the interfaces of the DNG shell. The magnitudes of the resulting normalized reactance values

$$\begin{aligned} X_{\rm norm}(r_{\rm obs}) =& \frac{2\omega\left[W_m(r_{\rm obs}) - W_e(r_{\rm obs})\right]}{P_{\rm rad}} \\ X_{\rm norm}^{\rm pos}(r_{\rm obs}) =& \frac{2\omega\left[W_m^{\rm pos}(r_{\rm obs}) - W_e^{\rm pos}(r_{\rm obs})\right]}{P_{\rm rad}} \end{aligned} \tag{39}$$

are shown in Fig. 15. As can be seen, the distance $r_{\rm obs} =$ m was sufficient for the normalized reactances to settle into

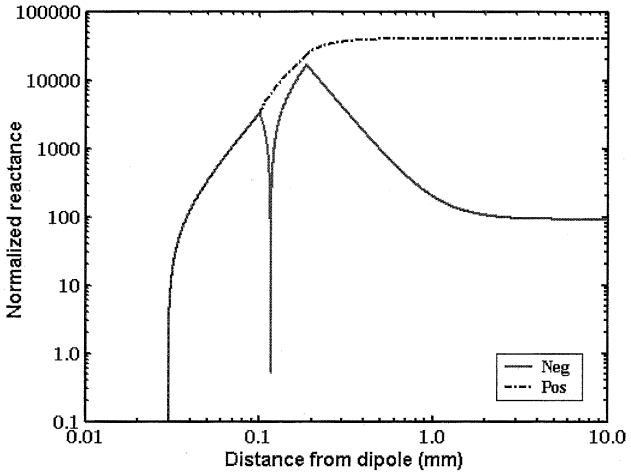

Fig. 15. Magnitude of the normalized reactance calculated directly from the energy expressions $W_{e,m}(r)$ (solid line) and from $W_{e,m}^{\rm pos}(r)$ (solid-dashed line) are shown as functions of the distance from the dipole antenna. The DNG shell with $(\varepsilon_2, \mu_2) = (-3\varepsilon_0, -3\mu_0)$ was defined with $r_1 = 100\ \mu$m and $r_2 = 185.8004\ \mu$m; the source frequency was 10 GHz.

their values corresponding to the limit $r_{\rm obs} \rightarrow \infty$. There are orders of magnitude difference between the result that took into account the negative signs of the permittivity and permeability values $X_{\rm norm}(r_{\rm obs})$ and the artificially constructed one $X_{\rm norm}^{\rm pos}(r_{\rm obs})$ that imposed absolute values for the permittivity and permeability everywhere. In particular, the measured value $X_{\rm norm}(r_{\rm obs})$ was $+91.396$ and the measured value of $X_{\rm norm}^{\rm pos}(r_{\rm obs})$ was -4.0546×10^4. The former shows excellent agreement in both magnitude and sign with the result calculated earlier using the complex power; the latter is simply inconsistent. Thus, (1)–(3) are consistent for the dipole-DNG shell system only if negative energies in the DNG region are taken into account.

Yet another possibility would be to avoid the negative energy issue entirely and deal only with the energies stored outside the DNG shell in the DPS region as:

$$W_e^{\rm outer}(r_{\rm obs}) = \frac{4\pi}{3}\int_{r_2}^{r_{\rm obs}} dr\, r^2 \left\{\frac{1}{2}\varepsilon_3 |e_r|^2 + \frac{1}{2}\varepsilon_3 |e_\theta|^2\right\}$$
$$W_m^{\rm outer}(r_{\rm obs}) = \frac{4\pi}{3}\int_{r_2}^{r_{\rm obs}} dr\, r^2 \left\{\frac{1}{2}\mu_3 |h_\phi|^2\right\} \quad (40)$$

If one were to calculate all of the reactance results from the complex power at r_2, i.e., only exterior to the DNG shell, one would obtain $X_R^{\rm DNG}(r_2) \simeq X_R^{\rm DPS}(r_2) \simeq X_{\rm norm}^{\rm outer}(r_{\rm obs}) \simeq 1.7 \times 10^4$, where $X_{\rm norm}^{\rm outer}(r_{\rm obs}) = 2\omega\,[W_m^{\rm outer}(r_{\rm obs}) - W_e^{\rm outer}(r_{\rm obs})]/P_{\rm rad}$ for $r_{\rm obs} = 10.0$ mm. That is, all values of the reactance are equivalent when they are calculated beyond the DNG shell (in Region 3), regardless of the parameters of the DNG shell. Therefore, measuring the reactance in Region 3 would not convey any meaningful correlation to changes in the radiated power caused by the DNG shell. The only correlation appears when Maxwell's equations are used directly, i.e., when (3) are used with no modifications and those "energy" terms are negative in a DNG region.

Note that if one considers the circuit equivalence in Fig. 6, the reactance changes its sign in the presence of the dual capacitance and inductance elements that represent the DNG metamaterial. In particular, the equation for the complex power associated with an *RLC* circuit

$$\frac{1}{2}VI^* = \frac{1}{2}II^*\left(R + j\omega L - j\frac{1}{\omega C}\right) \quad (41)$$

where the terms $V = ZI$, $P_r = (1/2)RII^*$, $W_m = (1/4)LII^*$, $W_e = (1/4)II^*/\omega^2 C$, allows one to extract the impedance immediately as

$$Z = \frac{P_r + 2j\omega(W_m - W_e)}{\frac{II^*}{2}}. \quad (42)$$

If the dual capacitance and inductance elements are introduced, the signs of the energy terms W_e and W_e become negative, and they must be preserved in order to obtain the correct overall reactance. This agrees with the observed change in sign of the reactance for the highly tuned, matched dipole-DNG shell system.

One might wonder whether these conclusions would be altered if the dispersive nature of a real DNG metamaterial were considered. If one assumed that the permittivity and permeability were dispersive, one would most probably calculate the total field energy with the well known expression (e.g., [7, pp. 14–17])

$$W_{\rm total}^{\rm dispersive} = \frac{1}{4}\iiint_V dV\ \left\{\partial_\omega\left[\omega\varepsilon(\omega)\right]\ \left|\vec{E}_\omega\right|^2 + \partial_\omega\left[\omega\mu(\omega)\right]\ \left|\vec{H}_\omega\right|^2\right\}. \quad (43)$$

However, as shown in [17], there are physical, causal DNG metamaterial models that yield negative energy values using (43). In contrast, the electromagnetic power flow calculations reported in [3], [17] that considered Poynting's theorem in the time domain:

$$\oiint_S dS(-\hat{n}_S) \bullet \left[\vec{E}(\vec{r},t) \times \vec{H}(\vec{r},t)\right]$$
$$= \partial_t\left\{\iiint_V dV\left[\frac{1}{2}\varepsilon_0\left|\vec{E}(\vec{r},t)\right|^2 + \frac{1}{2}\mu_0\left|\vec{H}(\vec{r},t)\right|^2\right]\right\}$$
$$+ \iiint_V dV\left[\vec{E}(\vec{r},t) \bullet \partial_t\vec{P}(\vec{r},t) + \mu_0\vec{M}(\vec{r},t) \bullet \partial_t\vec{H}(\vec{r},t)\right] \quad (44)$$

always showed that the average power flow was positive, i.e., positive electromagnetic field power flowing into a region was transferred to positive power associated with the fields and the metamaterial in that region. Thus, the total electromagnetic power in a DNG medium has been shown previously to be positive even for the cases in which the corresponding energy calculation was negative. Note that (44) does not attempt to introduce and use positive definite quantities, W_e and W_m, for

both the energies associated with the fields *and* the metamaterial. Rather, the power associated with the metamaterial is calculated with the time derivative changes of the polarization and magnetization fields themselves. Thus, if one chooses to introduce the energy quantities W_e and W_m and if they are negative, their existence does not violate our usual conservation of power theorem. One simply needs a proper interpretation of what they would represent to us.

We wish to emphasize that the introduction of the quadratic forms W_e and W_m is a traditional choice. The reactance and power calculations obtained through the complex Poynting's theorem actually do not depend on this choice. It is possible that the simple expressions for the field energies, (3), are not appropriate in the DNG cases because they are missing terms that would make them individually be positive, but would not change their difference. On the other hand, they may be correct as is.

What then might the frequency domain, time harmonic negative energy values mean? We have shown that the complex Poynting's theorem is satisfied only if they are taken into account. We believe that these negative energy terms are a direct result of the fact that the DNG properties can only exist after a field has interacted with the metamaterial system and has created the negative permittivity and permeability. This creation process is not reflected in the present steady state solution as it is in (44) which accounts for the source field creating the DNG properties through the associated time variations of the effective polarization and magnetization terms. The DNG shell does not magically produce energy from nothing. The negative energies here reflect the fact that if the excitation field were turned off, the DNG metamaterial would return to a DPS state, releasing the energy used to create the DNG state. This type of behavior was reported for the DNG metamaterials discussed in [3], [17].

There is precedence in physics for this proposed interpretation of the negative DNG shell energy. In particular, Dirac found both positive and negative energy states for his quantum mechanical particle equations [18]. He had to introduce the concept of holes to reconcile the possibility of the existence of these negative energy states. A hole (negative energy state) is formed by the excitation of an electron into a positive energy state. The recombination of an electron and a hole recovers that energy. We suggest that the DNG configuration in steady state is like the presence of a hole that has been created in a semiconductor by the emission of an electron.

VIII. Radiation Q for the Dipole-DNG Shell System

The fundamental limits on the radiation quality factor, Q, associated with electrically small antennas have been explored by many authors [5], [13]–[15], [19]–[22]. The most precise analyzes have defined the limiting radiation Q for antennas as the time-averaged, nonpropagating energy stored externally to the smallest sphere that could enclose the antenna divided by the antenna's real radiated power [19], [22]. Any realizable radiation Q would be greater than this value because additional energy would be stored within the enclosing sphere. The radiation Q, also defined as 2π times the ratio of the maximum energy stored to the total power lost per period, is a convenient quantity to describe, for instance, the bandwidth of the antenna when a driving circuit is matched to it. It is generally accepted that a high radiation Q value corresponds to a large amount of reactive energy stored near the antenna, hence, a correspondingly low value of the radiated power.

The minimum radiation Q attainable by an infinitesimal electric dipole, or similarly by the TM_{10} spherical mode with azimuthal symmetry, has been investigated the most thoroughly. The limit for the radiation Q in this case has been shown to be [13], [22]

$$Q = \frac{1+2(ka)^2}{(ka)^3\left[1+(ka)^2\right]} \simeq \frac{1}{(ka)^3} \text{ for } ka \ll 1. \tag{45}$$

Thus the radiation Q of a dipole in a DPS medium increases substantially as the electrical size of the antenna decreases. Note that while many authors present this result with the term $1+3(ka)^2$ in the numerator, we concur with the correction presented in [22] and given in (45) above. Finally, we note that the radiation Q for an electrically small antenna in a DPS medium is commonly approximated as [12], [15]

$$Q = \begin{cases} \frac{2\omega W_e}{P_{\mathrm{rad}}} & W_e \gg W_m \\ \frac{2\omega W_m}{P_{\mathrm{rad}}} & W_m \gg W_e \end{cases}. \tag{46}$$

From these equations, one immediately obtains $Q \simeq |X_R(a)|$ for an infinitesimal electric dipole immersed in a DPS medium. This result agrees with the fundamental limit (45) of the radiation Q when $ka \ll 1$. However, in the dipole-DNG shell case, the matching network interpretation implies that $W_e \sim W_m$; hence, this simplistic approach is no longer valid.

An explicit calculation of the radiation Q that leads to (45) in a DPS medium is obtainable by integrating the nonpropagating energy density over the region outside of the sphere of radius a [19], [22]. This approach was found to be the one best suited to the single mode, shell geometry under consideration. The nonpropagating energy in a spherical region extending from a sphere of radius a to ∞ is obtained by first calculating the time averaged total electromagnetic energy stored in that spherical region, i.e.,

$$\begin{aligned} W_{\mathrm{total}} &= W_e + W_m \\ &= \frac{4\pi}{3}\int_a^\infty dr r^2 \left\{ \frac{1}{2}\varepsilon |e_r|^2 + \frac{1}{2}\varepsilon |e_\theta|^2 + \frac{1}{2}\mu |h_\phi|^2 \right\}. \end{aligned} \tag{47}$$

Next the time averaged propagating energy is obtained by determining the field terms, $e_{\theta,\,rad}$ and $h_{\phi,\,\mathrm{rad}}$, that decay as r^{-1} and, hence, that cause the energy density to decay as r^{-2} as $r \to \infty$. Then one calculates the expression

$$W_{\mathrm{prop}} = \frac{4\pi}{3}\int_a^\infty dr\, r^2 \left\{ \frac{1}{2}\varepsilon |e_{\theta,\mathrm{rad}}|^2 + \frac{1}{2}\mu |h_{\phi,\mathrm{rad}}|^2 \right\}. \tag{48}$$

The nonpropagating energy is finally obtained as

$$W_{\mathrm{nonprop}} = W_{\mathrm{total}} - W_{\mathrm{prop}}. \tag{49}$$

The radiation Q is then determined as

$$Q = \frac{\omega\,|W_{\rm nonprop}|}{P_{\rm rad}}. \tag{50}$$

We note that (47) for the total electromagnetic energy and (48) for the total radiated electromagnetic energy are themselves infinite. However, their difference, (49), yields a finite quantity. Thus, the nonpropagating energy calculation is in effect a renormalization of the total energy in the volume V outside of the sphere of radius a.

To estimate the equivalent radiation Q for the dipole-DNG shell system, two forms of the propagating energy were calculated. The first is obtained directly from (48); it takes the explicit form

$$\begin{aligned} W_{\rm prop,W}(r_{\rm obs}) =& \frac{4\pi}{3}\int_a^{r_1} dr r^2 \left\{\frac{1}{2}\varepsilon_1 |e_{\theta,\rm rad}|^2 + \frac{1}{2}\mu_1 |h_{\phi,\rm rad}|^2\right\} \\ &+ \frac{4\pi}{3}\int_{r_1}^{r_2} dr\, r^2 \left\{\frac{1}{2}\varepsilon_2 |e_{\theta,\rm rad}|^2 + \frac{1}{2}\mu_2 |h_{\phi,\rm rad}|^2\right\} \\ &+ \frac{4\pi}{3}\int_{r_2}^{r_{\rm obs}} dr\, r^2 \left\{\frac{1}{2}\varepsilon_3 |e_{\theta,\rm rad}|^2 + \frac{1}{2}\mu_3 |h_{\phi,\rm rad}|^2\right\} \end{aligned} \tag{51}$$

where all of the permittivities and permeabilities take their actual values in their respective media. The second form is calculated directly from the radiated power as in [19], i.e., the propagating energy takes the form of the radial integral of the radiated power divided by the speed in the respective regions:

$$\begin{aligned} W_{\rm prop,P}(r_{\rm obs}) =& \frac{4\pi}{3}\int_a^{r_1} dr r^2 \left\{\sqrt{\varepsilon_1}\sqrt{\mu_1}\left[{\rm Re}\left(e_{\theta,\rm rad}\times h^*_{\phi,\rm rad}\right)\right]\right\} \\ &+ \frac{4\pi}{3}\int_{r_1}^{r_2} dr\, r^2 \left\{\sqrt{\varepsilon_2}\sqrt{\mu_2}\left[{\rm Re}\left(e_{\theta,\rm rad}\times h^*_{\phi,\rm rad}\right)\right]\right\} \\ &+ \frac{4\pi}{3}\int_{r_2}^{r_{\rm obs}} dr\, r^2 \left\{\sqrt{\varepsilon_3}\sqrt{\mu_3}\left[{\rm Re}\left(e_{\theta,\rm rad}\times h^*_{\phi,\rm rad}\right)\right]\right\}. \end{aligned} \tag{52}$$

The double square root form of the inverse wave speed used here accounts for its sign in the DNG shell. Both forms should give the same result for the nonpropagating energy (49) to be used in the radiation Q calculation (50). For comparison purposes we also introduce, as in the preceding section, the corresponding positive-only calculations for the propagating energy:

$$\begin{aligned} W^{\rm pos}_{\rm prop,W}(r_{\rm obs}) =& \frac{4\pi}{3}\int_a^{r_1} dr\, r^2 \left\{\frac{1}{2}|\varepsilon_1|\,|e_{\theta,\rm rad}|^2 + \frac{1}{2}|\mu_1|\,|h_{\phi,\rm rad}|^2\right\} \\ &+ \frac{4\pi}{3}\int_{r_1}^{r_2} dr\, r^2 \left\{\frac{1}{2}|\varepsilon_2|\,|e_{\theta,\rm rad}|^2 + \frac{1}{2}|\mu_2|\,|h_{\phi,\rm rad}|^2\right\} \\ &+ \frac{4\pi}{3}\int_{r_2}^{r_{\rm obs}} dr\, r^2 \left\{\frac{1}{2}|\varepsilon_3|\,|e_{\theta,\rm rad}|^2 + \frac{1}{2}|\mu_3|\,|h_{\phi,\rm rad}|^2\right\} \end{aligned}$$

$$\begin{aligned} W^{\rm pos}_{\rm prop,P}(r_{\rm obs}) =& \frac{4\pi}{3}\int_a^{r_1} dr\, r^2 \left\{\sqrt{|\varepsilon_1\mu_1|}\left[{\rm Re}\left(e_{\theta,\rm rad}\times h^*_{\phi,\rm rad}\right)\right]\right\} \\ &+ \frac{4\pi}{3}\int_{r_1}^{r_2} dr\, r^2 \left\{\sqrt{|\varepsilon_2\mu_2|}\left[{\rm Re}\left(e_{\theta,\rm rad}\times h^*_{\phi,\rm rad}\right)\right]\right\} \\ &+ \frac{4\pi}{3}\int_{r_2}^{r_{\rm obs}} dr\, r^2 \left\{\sqrt{|\varepsilon_3\mu_3|}\left[{\rm Re}\left(e_{\theta,\rm rad}\times h^*_{\phi,\rm rad}\right)\right]\right\}. \end{aligned} \tag{53}$$

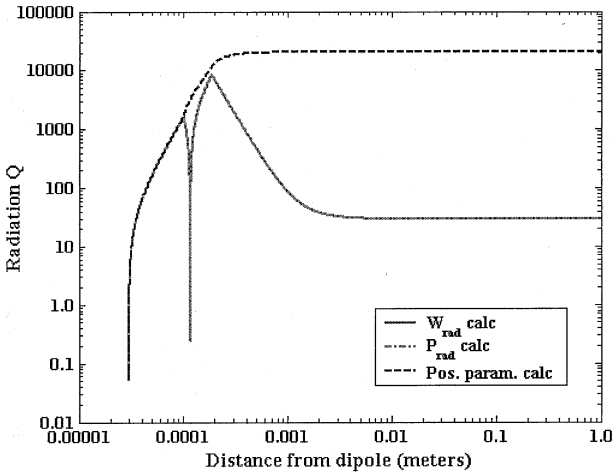

Fig. 16. The radiation Q was calculated with the nonpropagating energy expression for the case of the dipole surrounded by the DNG shell with $(\varepsilon_2,\mu_2) = (-3\varepsilon_0,-3\mu_0)$, $r_1 = 100\ \mu$m and $r_2 = 185.8004\ \mu$m. The radiation Q was calculated with the propagating radiated energy subtracted from the total field energy $W_{\rm total}$ (solid line) and with the propagating energy associated with the radiated power subtracted from $W_{\rm total}$ (solid-dashed line). As expected, they predicted identical values. The radiation Q was also calculated with the energy associated with the positive-only propagating energy (both the radiated energy and power forms) subtracted from the positive-only total field energy $W^{\rm pos}_{\rm total}$ (dashed line); it shows a dramatically different behavior.

We then calculate the radiation Q of the dipole-DNG shell system from (50) in the forms:

$$\begin{aligned} Q_W =& \frac{\omega\,|W_{\rm nonprop}|}{P_{\rm rad}} \\ =& \lim_{r_{\rm obs}\to\infty} \frac{\omega\,|W_{\rm total}(r_{\rm obs}) - W_{\rm prop,\,W}(r_{\rm obs})|}{P_{\rm rad}} \\ Q_P =& \frac{\omega\,|W_{\rm nonprop}|}{P_{\rm rad}} \\ =& \lim_{r_{\rm obs}\to\infty} \frac{\omega\,|W_{\rm total}(r_{\rm obs}) - W_{\rm prop,\,P}(r_{\rm obs})|}{P_{\rm rad}} \end{aligned} \tag{54}$$

$$\begin{aligned} Q^{\rm pos}_W =& \frac{\omega\,|W^{\rm pos}_{\rm nonprop}|}{P_{\rm rad}} \\ =& \lim_{r_{\rm obs}\to\infty} \frac{\omega\,\left|W^{\rm pos}_{\rm total}(r_{\rm obs}) - W^{\rm pos}_{\rm prop,\,W}(r_{\rm obs})\right|}{P_{\rm rad}} \\ Q^{\rm pos}_P =& \frac{\omega\,|W^{\rm pos}_{\rm nonprop}|}{P_{\rm rad}} \\ =& \lim_{r_{\rm obs}\to\infty} \frac{\omega\,\left|W^{\rm pos}_{\rm total}(r_{\rm obs}) - W^{\rm pos}_{\rm prop,\,P}(r_{\rm obs})\right|}{P_{\rm rad}} \end{aligned} \tag{55}$$

where the total energy expressions are simply

$$\begin{aligned} W_{\rm total}(r_{\rm obs}) =& W_e(r_{\rm obs}) + W_m(r_{\rm obs}) \\ W^{\rm pos}_{\rm total}(r_{\rm obs}) =& W^{\rm pos}_e(r_{\rm obs}) + W^{\rm pos}_m(r_{\rm obs}). \end{aligned} \tag{56}$$

All four of these radiation Q quantities were calculated for the DNG shell case with $(\varepsilon_2,\mu_2) = (-3\varepsilon_0,-3\mu_0)$, $r_1 = 100\ \mu$m, and $r_2 = 185.8004\ \mu$m when the source frequency was 10 GHz. The observation radius was taken to be $r_{\rm obs} = 1.0$ m. The calculation was broken up into three regions to increase its accuracy, i.e., the integration was divided into 30 000 intervals between a and $2r_2$, 30 000 intervals between $2r_2$ and 1.0 cm, and 30 000 intervals between 1.0 and 1.0 m. The radiation Q results are summarized in Fig. 16. The energy and power forms of the nonpropagating energy both lead, as expected, to the same value

of the radiation Q: 28.98. This quantity is 1.3912×10^5 times smaller than the free space value from (45): 4.0314×10^6. This decrease in the radiation Q is nicely consistent with the observed radiated power gain. On the other hand, the energy and power versions of the positive-only energy calculations both produced the same value of the radiation Q: 2.0308×10^4. This value is very inconsistent with the observed radiated power gain. Note, however, that even this latter value is 198.52 times smaller than the dipole-free space value.

The negative energy issues do dominate for the very narrow resonance cases that occur for the DNG shell being in close proximity to the dipole. The improvements over the free space dipole results are significant in these cases. The positive and negative energy differences are not very noticeable in the weak resonance cases that occur when the DNG shell is reasonably far away from the dipole. Moreover, the improvements, while being smaller, are not lost. For example, we found $Q_W = Q_P = 1.565 \times 10^3$ and $Q_W^{\text{pos}} = Q_P^{\text{pos}} = 1.583 \times 10^3$ for the DNG shell case with $(\varepsilon_2, \mu_2) = (-3\varepsilon_0, -3\mu_0)$ and with $r_1 = 1.0\ \text{mm}$ and $r_2 = 1.9661\ \text{mm}$. This means the radiation Q in this weak resonance case is 2.575×10^3 smaller than the free-space only value obtained from (45). We have found that for the $\varepsilon_r = \mu_r = -3$ cases, the crossover case where the negative energy contributions begin to be significant in comparison to the positive energy ones is the DNG shell with $r_1 = 565\ \mu\text{m}$ and $r_2 = 1074\ \mu\text{m}$.

Finally, we note that one should not immediately try to draw conclusions between the bandwidth of the dipole-DNG shell system and the observed radiation Q values, particularly with the presence of the negative energy terms. However, all of the results presented above indicate that the inner and outer shell radii have to be matched correctly with small tolerances or there will be a decrease in the performance. The dispersive DNG results indicate large variations in the performance with frequency and a realistic DNG material will have to be dispersive. Thus, it would appear that the dipole-DNG shell systems are finely tuned and, consequently, one would expect that their bandwidths would be narrow. Nonetheless, the bandwidth of the dipole-DNG shell system should be studied from a time domain point of view for proper results and their interpretation.

IX. Conclusion

The fields generated by an infinitesimal electric dipole in free space were compared to those generated by a dipole embedded in a DNG medium. It was observed that while the radiated power in both cases was equal, the reactive power in the DNG case was equal in magnitude but opposite in sign to the free space case. This property stimulated an investigation into the effect of placing a DNG shell around an infinitesimal electric dipole, in an attempt to "match" the dipole to free space.

Consequently, the problem of an infinitesimal electric dipole enclosed within a DNG shell was solved analytically. The equations associated with this configuration were presented, as were their numerical evaluations. Several DNG cases were considered. It was shown that in comparison to the dipole-free space case, the radiated power gain of the dipole-DNG shell system could be increased by orders of magnitude. The normalized reactance of the dipole-DNG shell configuration was shown to decrease by similar orders of magnitude. In addition, it was demonstrated that the radiated power gain (normalized reactance) could be increased (decreased) even further by making the permittivity and permeability of the DNG shell more negative or by decreasing its inner radius.

A lumped element circuit model of the dipole-DNG shell system confirmed that the system caused an increase in radiated power and a simultaneous decrease in the reactance. This approximate model revealed that it was possible to treat the presence of the DNG shell as a matching network. The fundamental TM_{10} spatial mode radiated by the dipole into free space was taken from below-cutoff to above-cutoff by a properly designed DNG shell, i.e., by creating an overall impedance that nearly matched that of free space.

The issues of the reactance and the radiation Q for the dipole-DNG shell system were explored. It was demonstrated through the complex Poynting's theorem that negative electromagnetic field energies are needed to describe correctly the phenomena associated with the dipole-DNG shell system. The nonpropagating energy expressions used in calculating the radiation Q were evaluated with negative material parameters and with their absolute value counterparts. Self-consistency of the radiated power, reactance and radiation Q required the presence of the negative energy terms. Arguments for why the appearance of the negative energy terms is not in violation of any basic physics principle and interpretations of what these terms represent physically were given. The results showed that the observed increase in the power radiated by a dipole-DNG shell configuration corresponded to a decrease of the normalized radiation Q, to values below the traditional Chu-limit.

Several metamaterial designs are currently under investigation to determine whether or not these theoretical results can be realized experimentally. Typical recent metamaterial analyzes and experiments have demonstrated that it is possible to achieve the relative permittivity and permeability values considered here or even more negative values. However, as noted throughout, nondispersive DNG metamaterials are unattainable. It is anticipated from a practical point of view that the presence of dispersion will have some type of negative impact on the extremely large resonance results as it does for focusing effects in DNG media. Even if this reduces the extreme results to substantially smaller values or reduces the modest values to a lesser degree, it is anticipated that the dipole-DNG shell results will still lead to nontrivial increases in the radiated power and corresponding decreases in the reactance and radiation Q. Nonetheless, the biggest difficulty in achieving these results appears to be the required small sizes of the DNG shells with low tolerances for variations in those sizes. To obtain the large enhancements shown here to be theoretically possible, much hard practical effort will have to be expended to realize metamaterial designs in ultra-small configurations. Nonetheless, the enormous potential payoff for extremely small, efficient radiators suggests that these DNG designs should be pursued aggressively.

Acknowledgment

One of the authors (R.W.Z) would like to thank Prof. G. Eleftheriades for several very interesting conversations concerning the equivalent circuit models for wave propagation in

DNG media and for sharing [16] and other more recent results during the Quantum Optics Workshop at the Kavli Institute for Theoretical Physics. The authors would like to thank one reviewer, Dr. A. Yaghjian, for his open, frank discussions on the original manuscript and its content; they led to a much improved revision. The authors would also like to thank Prof. N. Engheta for several stimulating discussions that helped improve the final version of this manuscript.

REFERENCES

[1] V. G. Veselago, "Electrodynamics of substances with simultaneously negative electrical and magnetic permeabilities," *Sov. Phys. Usp.*, vol. 10, pp. 5–13, Jan.-Feb. 1968.

[2] D. R. Smith, W. J. Padilla, D. C. Vier, S. C. Nemat-Nasser, and S. Schultz, "Composite medium with simultaneously negative permeability and permittivity," *Phys. Rev. Lett.*, vol. 84, pp. 4184–4187, May 2000.

[3] R. W. Ziolkowski and E. Heyman, "Wave propagation in media having negative permittivity and permeability," *Phys. Rev. E*, vol. 64, pp. 056 625/1–15, Nov. 2001.

[4] C. A. Balanis, *Antenna Theory Analysis and Design*, 2nd ed. New York: Wiley, 1997, ch. 4 & 11.

[5] R. F. Harrington, *Time-Harmonic Electromagnetic Fields*. New York: McGraw-Hill, 1961, ch. 6.

[6] R. E. Collin, *Foundations for Microwave Engineering*. New York: McGraw-Hill, 1966, pp. 28–33.

[7] ——, *Field Theory of Guided Waves*, 2nd ed. New York: IEEE, 1990, pp. 10–12.

[8] S. Ramo, J. R. Whinnery, and T. Van Duzer, *Fields and Waves in Communication Electronics*, 2nd ed. New York: Wiley, 1984, pp. 141–143.

[9] J. D. Jackson, *Classical Electrodynamics*, 2nd ed. New York: Wiley, 1975, pp. 241–244.

[10] D. M. Pozar, *Microwave Engineering*, 2nd ed. New York: Wiley, 1998, pp. 26–29.

[11] G. S. Smith, *An Introduction to Classical Electromagnetic Radiation*. Cambridge, U.K.: Cambridge University Press, 1997, pp. 94–98.

[12] M. Abramowitz and I. A. Stegun, *Handbook of Mathematical Functions*. New York: Dover, 1974, ch. 10.

[13] L. J. Chu, "Physical limitations of omnidirectional antennas," *J. Appl. Phys*, vol. 19, pp. 1163–1175, Dec. 1948.

[14] D. M. Grimes and C. A. Grimes, "Minimum Q of electrically small antennas: A critical review," *Microwave Opt. Tech. Lett.*, vol. 28, pp. 172–177, Feb. 2001.

[15] R. E. Collin, "Minimum Q of small antennas," *J. Electromagn. Waves Applicat.*, vol. 12, pp. 1369–1392, 1998.

[16] A. K. G. E. Eleftheriades, "Negative refractive index metamaterials supporting 2-D waves," *IEEE Int. Microwave Symp. Dig.*, vol. 2, pp. 1067–1070, June 2002.

[17] R. W. Ziolkowski, "Superluminal transmission of information through an electromagnetic metamaterial," *Phys. Rev. E*, vol. 63, p. 046 604, Apr. 2001.

[18] J. D. Bjorken and S. D. Drell, *Relativistic Quantum Mechanics*. New York: McGraw-Hill, 1964, ch. 5, pp. 63–75.

[19] R. E. Collin and S. Rothschild, "Evaluation of antenna Q," *IEEE Trans. Antennas Propagat.*, vol. AP-12, pp. 23–27, Jan. 1964.

[20] H. A. Wheeler, "Small antennas," *IEEE. Trans. Antennas Propagat.*, vol. AP-23, July 1975.

[21] R. C. Hansen, "Fundamental limitations in antennas," *Proc. IEEE*, vol. 69, pp. 170–181, Feb. 1981.

[22] J. S. McLean, "A re-examination of the fundamental limits on the radiation Q of electrically small antennas," *IEEE Trans. Antennas Propagat.*, vol. 44, pp. 672–676, May 1996.

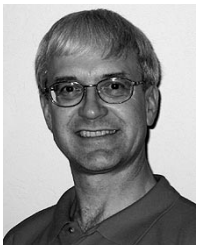

Richard W. Ziolkowski (M'97–SM'91–F'94) received the Sc.B. degree in physics (*magna cum laude*) with honors from Brown University, Providence, RI, in 1974 and the M.S. and Ph.D. degrees in physics from the University of Illinois at Urbana-Champaign, in 1975 and 1980, respectively.

He was a member of the Engineering Research Division, Lawrence Livermore National Laboratory, CA, from 1981 to 1990, and served as the leader of the Computational Electronics and Electromagnetics Thrust Area for the Engineering Directorate, from 1984 to 1990. He joined the Department of Electrical and Computer Engineering, University of Arizona, Tuscon, as an Associate Professor in 1990, and was promoted to Full Professor in 1996. His research interests include the application of new mathematical and numerical methods to linear and nonlinear problems dealing with the interaction of acoustic and electromagnetic waves with realistic materials and structures.

Prof. Ziolkowski is a Member of Tau Beta Pi, Sigma Xi, Phi Kappa Phi, the American Physical Society, the Optical Society of America, the Acoustical Society of America, and Commissions B (Fields and Waves) and D (Electronics and Photonics) of URSI (International Union of Radio Science). He was an Associate Editor for the IEEE TRANSACTIONS ON ANTENNAS AND PROPAGATION from 1993 to 1998. He served as the Vice Chairman of the 1989 IEEE/AP-S and URSI Symposium in San Jose, and as the Technical Program Chairperson for the 1998 IEEE Conference on Electromagnetic Field Computation in Tucson. He served as a member of the IEEE AP-S Administrative Committee (ADCOM) from 2000 to 2002. He is currently serving as Co-Guest Associate Editor with Prof. Nader Engheta for this IEEE TRANSACTIONS ON ANTENNAS AND PROPAGATION Special Issue on Metamaterials. For the US URSI Society, he served as Secretary for Commission B (Fields and Waves) from 1993 to 1996 and as Chairperson of the Technical Activities Committee from 1997 to 1999, and as Secretary for Commission D (Electronics and Photonics) from 2001 to 2002. He is currently serving as a Member-at-Large of the U.S. National Committee (USNC) of URSI and as a member of the International Commission B Technical Activities Committee. He was a Co-Guest Editor of the 1998 Special Issue of the *Journal of the Optical Society of America A* featuring Mathematics and Modeling in Modern Optics. He was a Co-Organizer of the Photonics Nanostructures Special Symposia at the 1998, 1999, and 2000 OSA Integrated Photonics Research (IPR) Topical Meetings. He served as the Chair of the IPR subcommittee IV, Nanostructure Photonics, in 2001. He was awarded the Tau Beta Pi Professor of the Year Award in 1993 and the IEEE and Eta Kappa Nu Outstanding Teaching Award in 1993 and 1998. He also holds the title of Sensei with a Nidan rank in Matsunoryu Goshin Jujitsu and a Shodan rank in Kajukenbo.

Allison D. Kipple (S'00) received the B.S. degree in aerospace engineering (*summa cum laude*) from the University of Colorado, Boulder, in 1992 and the M.S. degree in electrical and computer engineering from the University of Arizona, Tuscon, in 2000.

From 1988 to 1993, she was a Research Assistant with the Laboratory for Atmospheric and Space Physics, Boulder. She was a Calibration Engineer at the Alaska Synthetic Aperture Radar Facility, from 1995 to 1998. She has served as a Technical Investigator with the U.S. Army Electronic Proving Ground since 2001. Her research interests include the effects of metamaterials on antenna performance.

Ms. Kipple is a member of the IEEE Antennas and Propagation and Education Societies and the American Society for Engineering Education. She received a local IEEE Engineer of the Year award in 2003 and has been awarded Graduate College and NASA Space Grant Graduate Fellowships.